

Molecular dynamics simulation of the transformation of Fe-Co alloy by machine learning force field based on atomic cluster expansion

Yongle Li^{1,*}, Feng Xu¹, Long Hou¹, Luchao Sun², Haijun Su³, Xi Li^{1,4}, Wei Ren^{1,*}

¹ *Physics Department, State Key Laboratory of Advanced Special Steels, Materials Genome Institute, International Centre for Quantum and Molecular Structures, Shanghai University, Shanghai 200444, China*

² *Shenyang National Laboratory for Materials Science, Institute of Metal Research, Chinese Academy of Sciences, Shenyang 110016, China*

³ *State Key Laboratory of Solidification Processing, Northwestern Polytechnical University, Xi'an 710072, China*

⁴ *Shanghai Key Lab of Advanced High-temperature Materials and Precision Forming, Shanghai Jiao Tong University, Shanghai 200240, PR China*

**Emails: yongleli@shu.edu.cn; renwei@shu.edu.cn*

Abstract

The force field describing the calculated interaction between atoms or molecules is the key to the accuracy of many molecular dynamics (MD) simulation results. Compared with traditional or semi-empirical force fields, machine learning force fields have the advantages of faster speed and higher precision. We have employed the method of atomic cluster expansion (ACE) combined with first-principles density functional theory (DFT) calculations for machine learning, and successfully obtained the force field of the binary Fe-Co alloy. Molecular dynamics simulations of Fe-Co alloy carried out using this ACE force field predicted the correct phase transition range of Fe-Co alloy.

Key words: Molecular dynamics, Atomic cluster expansion, Fe-Co Alloy, Density functional theory, Phase transition, Force field

Introduction

Alloy is usually a substance with metallic properties synthesized by two or more metal elements, or metal and non-metal elements through a specific method. According to the types of elements contained in the alloy, it can be divided into binary alloys, ternary alloys or multi-element alloys^[1,2]. The research on the phase transition of alloy materials has always been the focus of many scientific fields. Although numerous simulations of melting and solidification of alloys have been reported, progress in this area has been rather slow^[3,4].

Molecular dynamics (MD) is an effective means of simulating the phase transition of alloy materials, and molecular dynamics is widely applied in various fields such as physics, chemistry, biology and materials science^[5-8]. At present, there are many methods for simulating the phase transformation of alloys by using molecular dynamics^[9]. But the correctness of the molecular dynamics simulation results is largely limited by the precision of the chosen force field, which should benefit from the rapid development of empirical and semi-empirical many-body potentials describing metallic systems.

At present, the force fields that can be selected in the simulation of alloy materials include the Lennard-Jones (LJ) potential^[10], embedded atom method (EAM) potential^[11] and modified embedded atom method (MEAM) potential^[12, 13], etc. Given the diversity and complexity of elements contained in alloys, the use of machine learning to fit force field parameters is faster, more promising, and hopefully more widely applicable than traditional force field development. Therefore, this paper uses the method of atomic cluster expansion (ACE)^[14, 15] combined with first-principles density functional theory (DFT) calculations for machine learning to fit a force field that can be used for binary Fe-Co alloys. The melting and solidification mechanism of the binary Fe-Co alloy is revealed through the ACE force field, which expands the application of the ACE force field.

Methods

Atomic cluster expansion is a complete descriptor that can describe the local atomic environment of multicomponent materials. Some expressions for multivariate systems and non-orthogonal basis functions are given. Interatomic potentials with comparable precision to state-of-the-art machine learning potentials can be obtained by nonlinear functions from atomic clusters, which should converge to the precision of millielectron volt (meV). The principle of atomic cluster expansion is that the energy of the i -th atom is expressed as the coordinates related to other atoms^[14].

$$E_i(\mathbf{r}_1, \mathbf{r}_2, \dots, \mathbf{r}_N) = \sum_{\nu} c_{\nu}^{(1)} A_{i\nu} + \sum_{\nu_1 \geq \nu_2} c_{\nu_1 \nu_2}^{(2)} A_{i\nu_1} A_{i\nu_2} + \sum_{\nu_1 \geq \nu_2 \geq \nu_3} c_{\nu_1 \nu_2 \nu_3}^{(3)} A_{i\nu_1} A_{i\nu_2} A_{i\nu_3} + \dots \quad (1)$$

$$A_{i\nu} = \sum_j \phi_{\nu}(\mathbf{r}_{ji}) \quad (2)$$

where c is the expansion coefficient and $A_{i\nu}$ is the projection of the basis function on the atomic density.

Before fitting the ACE force field, we need to do preparatory work to create some sufficiently disordered systems, the atomic positions of which are random. For the selected systems, we obtain their energy, virial^[16] and other information through first-principles density functional theory calculations. The DFT calculations were carried out using the Vienna Ab initio Simulation Package (VASP)^[17], with projection-based augmented wave pseudopotentials^[18], and Perdew-Burke-Ernzerhof (PBE)^[19] generalized gradient approximation functional. In all calculations, the plane wave cutoff energy was chosen to be 400 eV, the atomic force convergence criterion was 0.01 eV·Å⁻¹, the energy convergence criterion was 10⁻⁶ eV, and the Brillouin zone was sampled with 13 × 13 × 13 k-points in a Monkhorst-Pack grid. After preparing various information of the system, we use the toolkit atomic simulation environment (ASE)^[20] to integrate based on the python programming language.

The initial structure is obtained by constructing supercell of body-centered cubic (bcc) Fe-Co alloy with periodic boundary conditions. The ratio of Fe atoms to Co atoms is 1:1. As shown in Fig. 1, the established 10 × 10 × 10, 20 × 20 × 20, 30 × 30 × 30, and 37 × 37 × 37 Fe-Co alloy supercells of the volumes 28.4 × 28.4 × 28.4 Å³, 56.8 ×

$56.8 \times 56.8 \text{ \AA}^3$, $85.2 \times 85.2 \times 85.2 \text{ \AA}^3$, and $105.08 \times 105.08 \times 105.08 \text{ \AA}^3$ contain 2,000, 16,000, 54,000, and 101,306 atoms respectively. The MD simulation of $37 \times 37 \times 37$ Fe-Co alloy supercell using the ACE force field is done with the Large-scale Atomic Molecular Massively Parallel Simulator (LAMMPS)^[21]. The volume, density and other physical properties of this supercell at 300 K were simulated. In addition, four Fe-Co alloy supercells of different sizes were subjected to MD simulations under the isothermal-isobaric (NPT) ensemble. A Nosé-Hoover chain thermostat^[22, 23] was used to control the system temperature and an Andersen method barostat^[24] was used to control the pressure (1 atmosphere). The melting process of Fe-Co alloy supercells from 1 K to 2500 K is simulated with a time step of 1 fs and a heating rate of 0.5 K/ps^[25]. The Velocity-Verlet algorithm^[26] is used to solve the propagation classical equation of motion, and sample the real-time position and velocity of particles. Equilibrium simulations were performed at 1 K for 10 ps before the system was heated up. In addition, the solidification process of $37 \times 37 \times 37$ Fe-Co alloy supercell cooling from 2500 K to 1000 K was simulated under the same conditions. Before the system cools down, equilibrium was simulated at 2500 K for 100 ps to ensure the system was in the liquid state. The Visual Molecular Dynamics (VMD)^[27] package and the Open Visualization Tool (OVITO) package were used for structure monitoring and trajectory analysis of various output data generated in MD simulations.

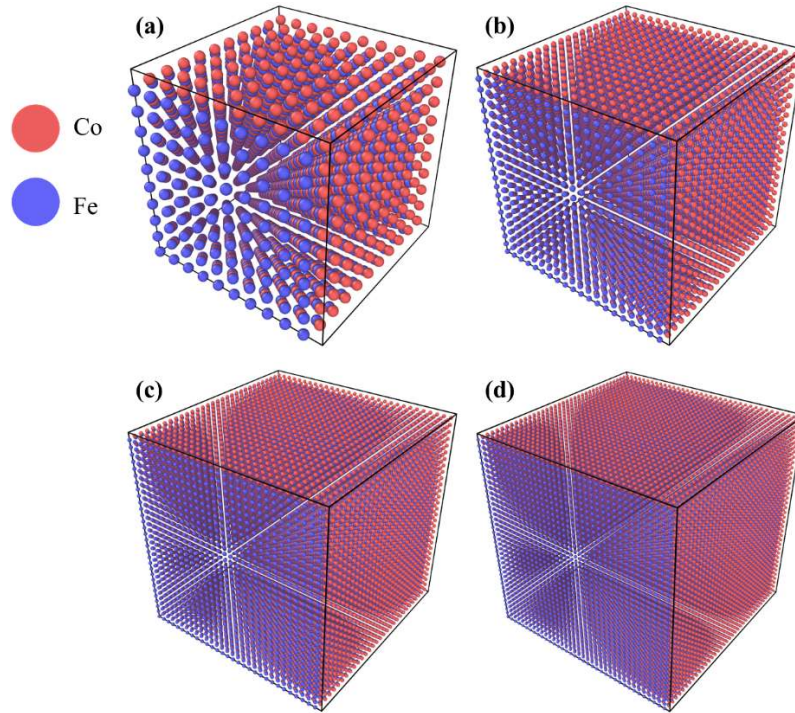


Fig. 1. (a) supercell structure of Fe-Co alloy $10 \times 10 \times 10$, (b) supercell structure of Fe-Co alloy $20 \times 21 \times 20$, (c) supercell structure of Fe-Co alloy $30 \times 30 \times 30$ and (d) supercell structure of Fe-Co alloy $37 \times 37 \times 37$.

Results and discussion

Verification of ACE force field at 300 K

In order to verify the correctness of the ACE force field, we simulated various properties of the $37 \times 37 \times 37$ Fe-Co alloy supercell at 300 K, including volume, density and energy. As shown in Fig. 2, the $37 \times 37 \times 37$ Fe-Co alloy is heated starting at ultralow temperature 1 K to 300 K at 0.5 K/ps and equilibrated at 300 K for 10 ns after a period of equilibrium. The insets zoom in the results when the temperature is goes up. In the simulation of equilibrium at 300 K for 10 ns, its fluctuation is found to be reasonably small. At this time, the temperature, volume, density and energy of the $37 \times 37 \times 37$ Fe-Co alloy supercell are recorded in Table 1, which are in excellent agreement with the experimental values^[28].

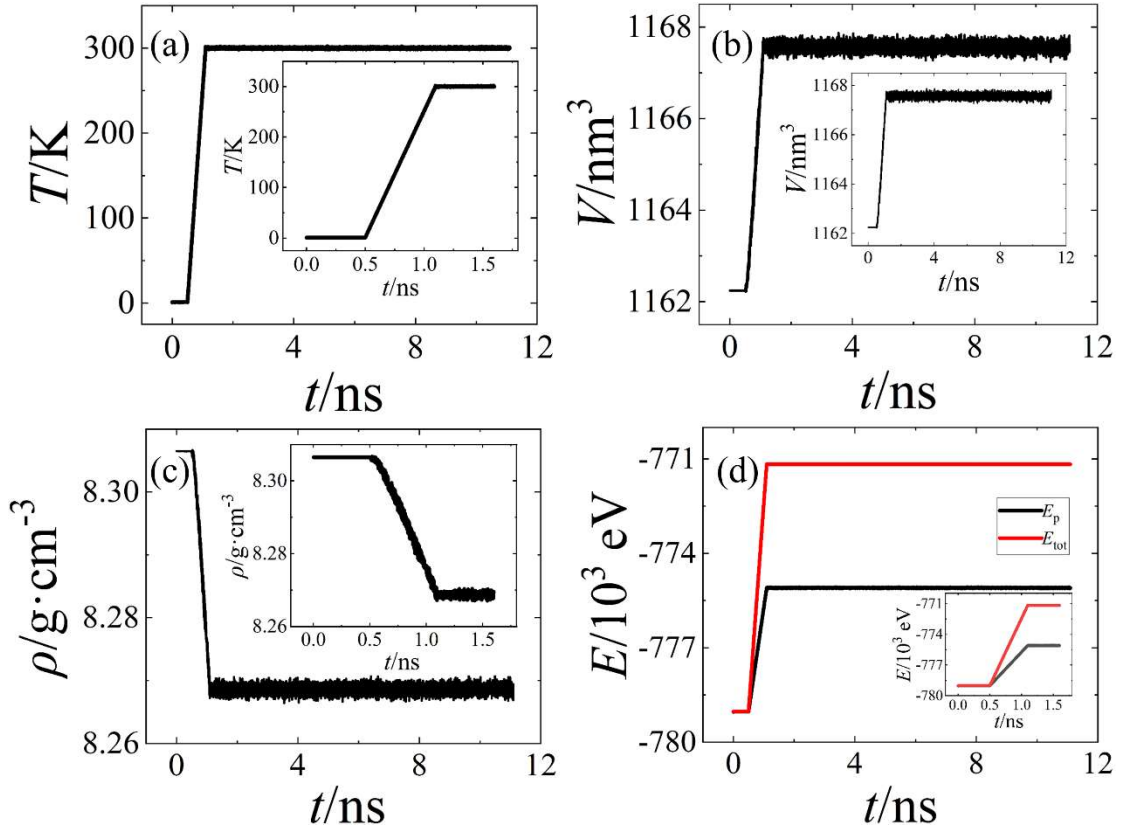


Fig 2. (a) Temperature; (b) volume; (c) density and (d) energy change curves with evolution time of $37 \times 37 \times 37$ Fe-Co alloy supercell structure using ACE force field for molecular dynamics. The insets are the enlarged pictures of the heating stage.

Table 1. Parameter values and fluctuations of $37 \times 37 \times 37$ Fe-Co alloy supercell from molecular dynamics equilibrium under ACE force field and experimental values

of related parameters.

| Property | This Work | Fluctuation | Experimental ^[28] |
|------------------------------|-----------|-------------|------------------------------|
| Temperature (K) | 300 | ± 2 | |
| Volume (nm ³) | 1167.56 | ± 0.31 | 1172.57 |
| Density (g/cm ³) | 8.269 | ± 0.002 | 7.9 - 8.0 |
| Potential Energy (eV) | -775097 | ± 26 | |
| Total Energy (eV) | -771168 | ± 4 | |

We have also used the ACE force field to simulate the bulk elastic modulus of Fe-Co alloy at 300 K, and searched for the structure with the lowest unit cell energy of Fe-Co alloy by changing the lattice parameters. Due to the relatively small number of atoms in the unit cell, there may be size-induced errors in the simulation results, so we expanded the Fe-Co alloy cell to $37 \times 37 \times 37$. The Fe-Co alloy equilibrium lattice parameter (at the minimal point of Fig. 3) is denoted by a_0 , and the potential energy of the unit cell is denoted by E_p . The bulk modulus^[29] is defined as follows:

$$B \equiv -\frac{dP}{dV/V} \quad (3)$$

V and P correspond to the volume and pressure, respectively. And for a cubic unit cell we have:

$$P = -\frac{d\varepsilon}{dV} = -\frac{M}{3a^2} \frac{dE}{da} \quad (4)$$

At this condition:

$$B = \frac{M}{9a_0} \left. \frac{d^2E}{da^2} \right|_{a_0} \quad (5)$$

where M in the formula is the number of atoms in the cubic unit cell.

As shown in Fig 3, we simulated the variation of the unit cell potential energy of the Fe-Co alloy upon changing the lattice parameter. At the minimum, the equilibrium lattice parameter $a_0 = 2.842 \text{ \AA}$, and the unit cell potential energy $E_p = -15.38 \text{ eV}$. We performed a fifth-order nonlinear fitting on the potential energy of the unit cell corresponding to different lattice parameters, and obtained the expression of potential energy and lattice parameters as: $E = b_0 + b_1a^1 + b_2a^2 + b_3a^3 + b_4a^4 + b_5a^5$. From

formula (5), we obtained a bulk modulus of $2.376 \text{ eV}/\text{\AA}^3$ for the Fe-Co alloy which is close to the experimental value^[30].

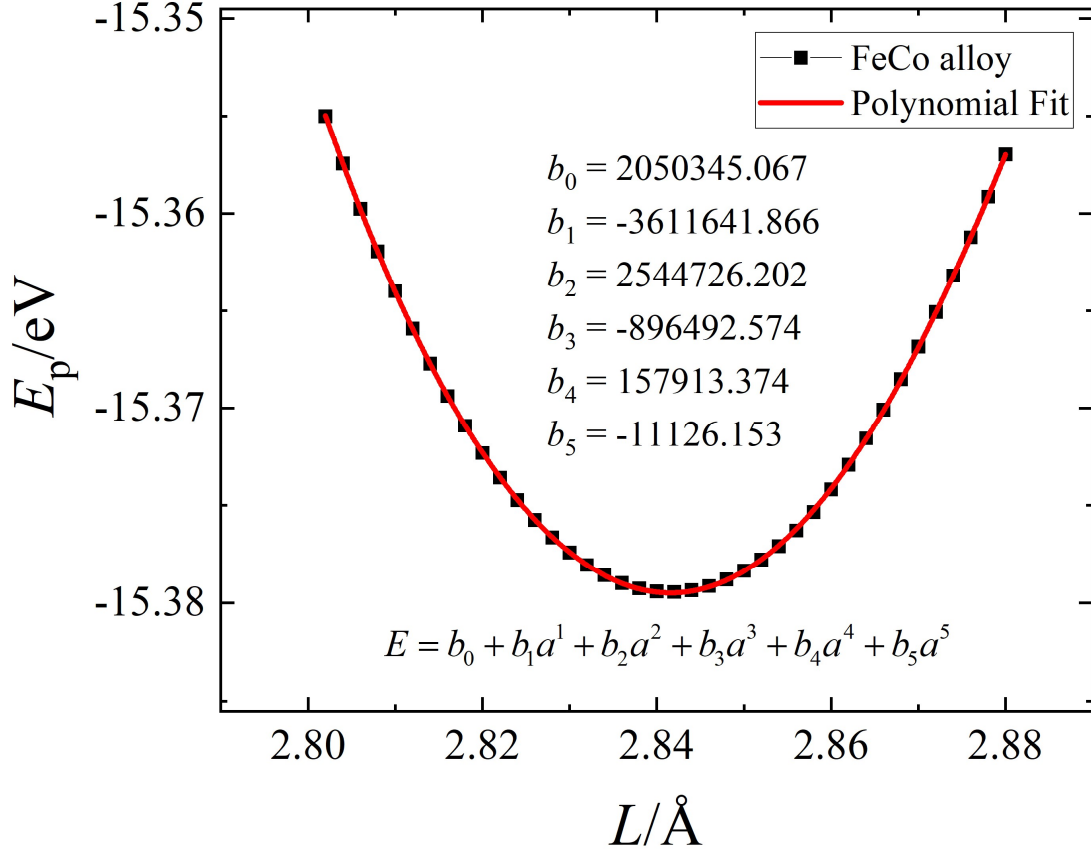


Fig. 3. The variation curve of unit cell potential energy of Fe-Co alloy with lattice parameters.

Phase transitions - Melting and Freezing points

We simulated the heating up of $10 \times 10 \times 10$, $20 \times 20 \times 20$, $30 \times 30 \times 30$ and $37 \times 37 \times 37$ Fe-Co alloy supercells from 1 K to 2500 K, respectively. As shown in Fig. 4, the melting point range of the system can be judged by observing the volume change with temperature. And we found that with the increase of the number of atoms in the system, the fluctuation of the melting point becomes smaller and smaller. Taken the $37 \times 37 \times 37$ Fe-Co alloy supercell as an example, its melting point is about 1766 K, which agrees very well with the experimental values and the results of other force field simulations. The melting points and their fluctuations for Fe-Co alloy supercells of different sizes, as well as the experimental values and the results simulated by other force fields are listed in Table 2.

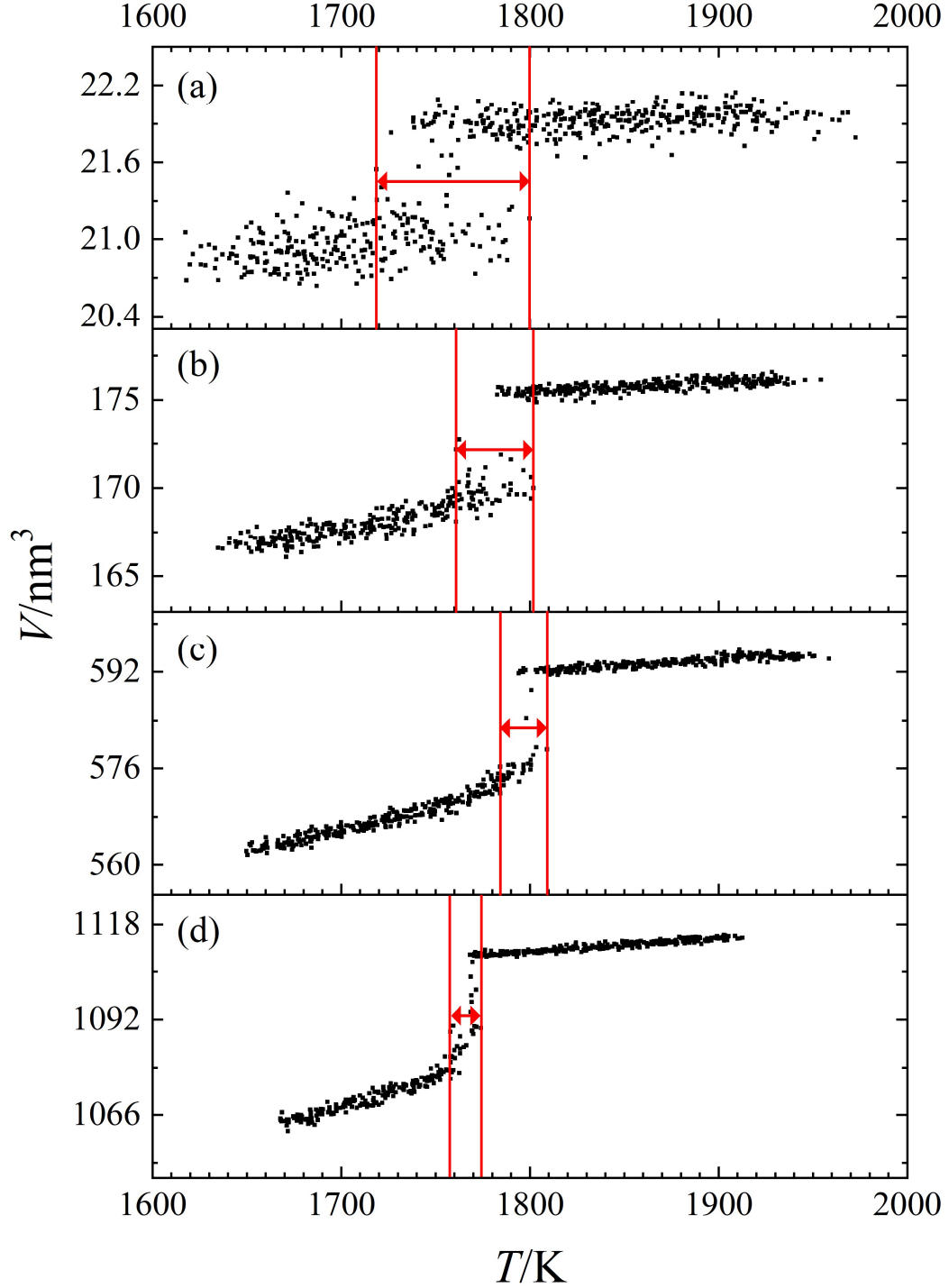


Fig. 4. (a) to (d) are the change in volume with temperature near the melting point during warming up of $10 \times 10 \times 10$, $20 \times 20 \times 20$, $30 \times 30 \times 30$ and $37 \times 37 \times 37$ Fe-Co alloy supercells. The red lines indicate the phase transition interval.

Table 2. Melting points and fluctuations of Fe-Co alloy supercells with different sizes using ACE force field, as well as experimental values and other force field simulation result.

| Size of the system | Melting point (K) | Fluctuation (K) |
|-------------------------------------|-------------------|-----------------|
| This Work_ $10 \times 10 \times 10$ | 1763 | ± 37 |
| This Work_ $20 \times 20 \times 20$ | 1781 | ± 20 |
| This Work_ $30 \times 30 \times 30$ | 1796 | ± 13 |
| This Work_ $37 \times 37 \times 37$ | 1766 | ± 8 |
| Experimental ^[31] | 1727,1724 | |
| Experimental ^[32] | 1750 | |
| MEAM ^[33] | 1700 | |

In order to understand the phase transformation mechanism of Fe-Co alloy in depth, we present the radial distribution function (RDF) $g(r)$ ^[34-36] of different temperature for $37 \times 37 \times 37$ Fe-Co alloy supercell during the heating process. The first peak in RDF represents the average number of atoms at the nearest neighbors of the target atom, and the second peak represents the average number of atoms at the next-nearest neighbors. When the Fe-Co alloy is melted, as in a liquid state, such phase only has short-range order. Therefore, the RDF of Fe-Co alloy after melting appears featureless after the nearest neighbor, and the peaks are wide and smooth. As the thermal motion of atoms becomes more and more intense with the increase of temperature, the heights of wave crests become lower and lower, while the wave peaks become wider and wider. In Fe-Co alloy with a bcc structure with a ratio of Fe:Co atomic numbers of 1:1, the nearest neighbor atoms of the body-centered atoms are located at the 8 vertices of the cubic unit cell, and the second nearest neighbor is the center of the adjacent unit cell. As shown in Fig 5, during the heating process, we found that as the temperature increased, the first peak began to decrease slowly, and the second split peak gradually became smoother, which means that the system is undergoing a phase transition.

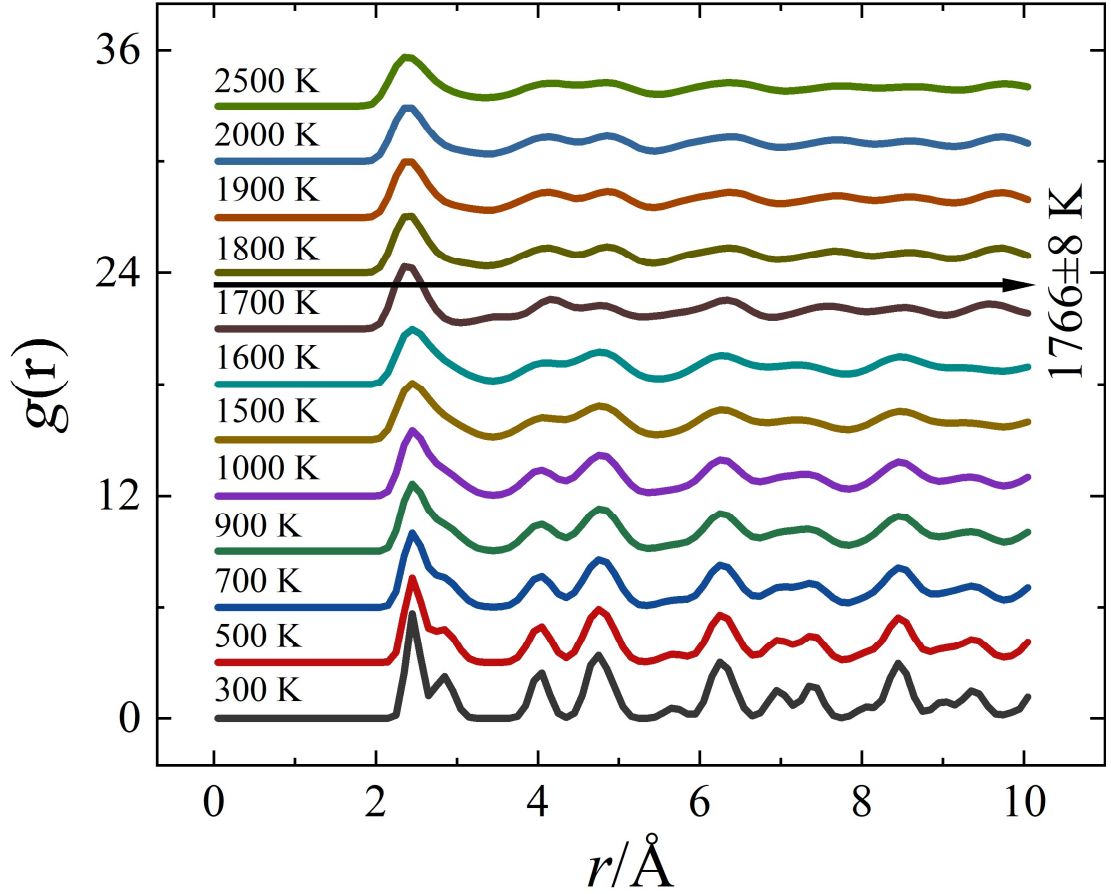


Fig. 5. Radial distribution function of Fe-Co alloy $37 \times 37 \times 37$ supercell at different temperatures.

As shown in Fig 6(a), we also used the ACE force field to simulate the cooling process (same rate as heating 0.5 K/ps) of the $37 \times 37 \times 37$ Fe-Co alloy supercell from 2500 K to 1200 K. Similarly, the freezing point of Fe-Co alloy is about 1665 K and the fluctuation is 5 K by observing the volume change with temperature. From Fig 6, we found that the volume, density and potential energy of the Fe-Co alloy near the phase transition point all behave to form closed loop of hysteresis.

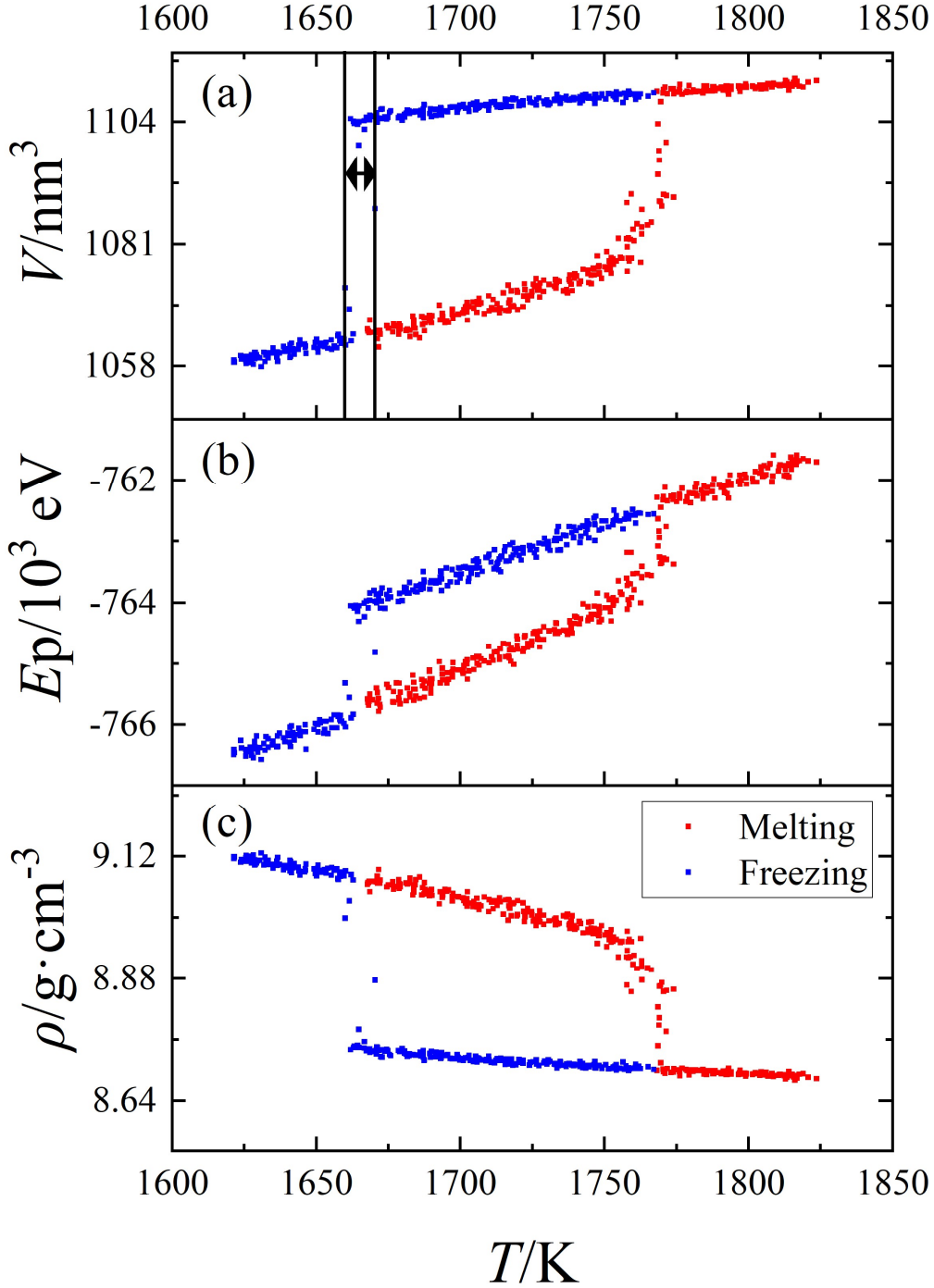


Fig. 6. Hysteresis loops of the (a) volume, (b) density and (c) potential energy of the $37 \times 37 \times 37$ Fe-Co alloy supercell versus temperature. The black lines indicate the phase transition interval.

As shown in Table 3, we found that the solidification and melting of metals or alloys are actually asymmetrical^[4], and the freezing point is smaller than the melting point. According to the classical nucleation theory^[37, 38], this is because the liquid system will be subcooled^[39, 40] during the solidification process and the interface where

the new phase appears will prevent the solidification from nucleation, and conversely, the equilibrium of surface energy at the interface between the phase and the phase during the melting process will prevent the solid from melting, so the melting and freezing points are not symmetrical and slightly different in temperature.

Table 3. Melting point and freezing point of $37 \times 37 \times 37$ Fe-Co alloy supercell and their fluctuations

| Properties | Temperature (K) | Fluctuation (K) |
|----------------|-----------------|-----------------|
| Melting point | 1766 | ± 8 |
| Freezing point | 1665 | ± 5 |

Conclusion

In this work, we have successfully fitted the force field of the binary Fe-Co alloy by machine learning combined with atomic cluster expansion and the first-principles density functional theory. The properties of Fe-Co alloy at 300 K were simulated by using the ACE force field, and the correctness of the obtained parameters was verified. From the ACE force field molecular dynamics, the melting point of Fe-Co alloy is 1766 ± 8 K, and the freezing point is 1665 ± 5 K. The hysteresis of the melting and freezing points of the Fe-Co alloy was found, which is consistent with the classical nucleation theory. The ACE force field is easier to fit than the traditional empirical and semi-empirical multi-body force fields, which may widely expand its application.

Acknowledgements

This work was supported by the National Natural Science Foundation of China (No. 22173057, 52130204, 12074241, and 11929401), Science and Technology Commission of Shanghai Municipality (Grants No. 21JC1402700, No. 20501130600, No. 20QA1401000, No. 21JC1402600, and No. 22XD1400900), High Performance Computing Center, Shanghai University, and Key Research Project of Zhejiang Laboratory (Grant No. 2021PE0AC02).

References

1. Habashi, F., *Alloys: preparation, properties, applications*. John Wiley & Sons: 2008.
2. Hume-Rothery, W., The structure of metals and alloys. *Indian Journal of Physics* **1969**, *11*, 74-74.
3. Cantor, B.; Chang, I. T. H.; Knight, P.; Vincent, A. J. B., Microstructural development in equiatomic multicomponent alloys. *Materials Science and Engineering: A* **2004**, *375-377*, 213-218.
4. Chattopadhyay, K.; Goswami, R., Melting and superheating of metals and alloys. *Progress in Materials Science* **1997**, *42* (1-4), 287-300.
5. Schiøtz, J.; Di Tolla, F. D.; Jacobsen, K. W., Softening of nanocrystalline metals at very small grain sizes. *Nature* **1998**, *391* (6667), 561-563.
6. Faux, D. A., Molecular dynamics studies of sodium diffusion in hydrated Na⁺-Zeolite-4A. *The Journal of Physical Chemistry B* **1998**, *102* (52), 10658-10662.
7. Yu-Hua, W.; Fu-Xin, Z.; Yue-Wu, L., Molecular dynamics simulation of microstructure of nanocrystalline copper. *Chinese Physics Letters* **2001**, *18* (3), 411.
8. Sun, H., Prediction of fluid densities using automatically derived VDW parameters. *Fluid phase equilibria* **2004**, *217* (1), 59-76.
9. Zhang, Y.; Maginn, E. J., A comparison of methods for melting point calculation using molecular dynamics simulations. *J Chem Phys* **2012**, *136* (14), 144116.
10. Heinz, H.; Vaia, R. A.; Farmer, B. L.; Naik, R. R., Accurate Simulation of Surfaces and Interfaces of Face-Centered Cubic Metals Using 12-6 and 9-6 Lennard-Jones Potentials. *The Journal of Physical Chemistry C* **2008**, *112* (44), 17281-17290.
11. Daw, M. S.; Baskes, M. I., Embedded-atom method: Derivation and application to impurities, surfaces, and other defects in metals. *Physical Review B* **1984**, *29* (12), 6443-6453.
12. Baskes, M. I., Modified embedded-atom potentials for cubic materials and impurities. *Phys Rev B Condens Matter* **1992**, *46* (5), 2727-2742.
13. Lee, B.-J.; Baskes, M. I., Second nearest-neighbor modified embedded-atom-method potential. *Physical Review B* **2000**, *62* (13), 8564-8567.
14. Drautz, R., Atomic cluster expansion for accurate and transferable interatomic potentials. *Physical Review B* **2019**, *99* (1).
15. Dusson, G.; Bachmayr, M.; Csányi, G.; Drautz, R.; Etter, S.; van der Oord, C.; Ortner, C., Atomic cluster expansion: Completeness, efficiency and stability. *Journal of Computational Physics* **2022**, *454*, 110946.
16. Thompson, A. P.; Plimpton, S. J.; Mattson, W., General formulation of pressure and stress tensor for arbitrary many-body interaction potentials under periodic boundary conditions. *J Chem Phys* **2009**, *131* (15), 154107.
17. Hafner, J., Ab-initio simulations of materials using VASP: Density-functional theory and beyond. *Journal of computational chemistry* **2008**, *29* (13), 2044-2078.
18. Kresse, G.; Joubert, D., From ultrasoft pseudopotentials to the projector augmented-wave method. *Physical review b* **1999**, *59* (3), 1758.
19. Perdew, J. P.; Burke, K.; Ernzerhof, M., Generalized gradient approximation made simple. *Physical review letters* **1996**, *77* (18), 3865.
20. Hjorth Larsen, A.; Jorgen Mortensen, J.; Blomqvist, J.; Castelli, I. E.; Christensen, R.; Dulak, M.; Friis, J.; Groves, M. N.; Hammer, B.; Hargus, C.; Hermes, E. D.; Jennings, P. C.; Bjerre Jensen, P.; Kermode, J.; Kitchin, J. R.; Leonhard Kolsbjerg, E.; Kubal, J.; Kaasbjerg, K.; Lysgaard, S.; Bergmann Maronsson, J.; Maxson, T.; Olsen, T.; Pastewka, L.; Peterson, A.;

- Rostgaard, C.; Schiotz, J.; Schutt, O.; Strange, M.; Thygesen, K. S.; Vegge, T.; Vilhelmsen, L.; Walter, M.; Zeng, Z.; Jacobsen, K. W., The atomic simulation environment—a Python library for working with atoms. *J Phys Condens Matter* **2017**, *29* (27), 273002.
21. Plimpton, S., Fast Parallel Algorithms for Short-Range Molecular Dynamics. *Journal of Computational Physics* **1995**, *117* (1), 1-19.
 22. Hoover, W. G., Canonical dynamics: Equilibrium phase-space distributions. *Phys Rev A Gen Phys* **1985**, *31* (3), 1695-1697.
 23. Nosé, S., A unified formulation of the constant temperature molecular dynamics methods. *The Journal of Chemical Physics* **1984**, *81* (1), 511-519.
 24. Grimme, S.; Antony, J.; Ehrlich, S.; Krieg, H., A consistent and accurate ab initio parametrization of density functional dispersion correction (DFT-D) for the 94 elements H-Pu. *J Chem Phys* **2010**, *132* (15), 154104.
 25. Yuqing, L.; Wenbin, F.; Xi, L.; Wei, R.; Yongle, L., Nucleation Mechanism of Iron in an External Magnetic Field. *Chinese Journal of Chemical Physics* **2021**, *34* (6), 843-849.
 26. Bussi, G.; Donadio, D.; Parrinello, M., Canonical sampling through velocity rescaling. *J Chem Phys* **2007**, *126* (1), 014101.
 27. Humphrey, W.; Dalke, A.; Schulten, K., VMD: visual molecular dynamics. *Journal of molecular graphics* **1996**, *14* (1), 33-38.
 28. Sundar, R.; Deevi, S., Soft magnetic FeCo alloys: alloy development, processing, and properties. *International materials reviews* **2005**, *50* (3), 157-192.
 29. Jamal, M.; Jalali Asadabadi, S.; Ahmad, I.; Rahnamaye Aliabad, H. A., Elastic constants of cubic crystals. *Computational Materials Science* **2014**, *95*, 592-599.
 30. Belousov, O.; Palii, N., Concentration and temperature dependences of the elastic properties of quenched Fe-Co and FeCo-2V alloys. *Russian Metallurgy (Metally)* **2009**, *2009* (1), 41-49.
 31. Rodriguez, J. E.; Matson, D. M., Thermodynamic modeling of the solidification path of levitated Fe-Co alloys. *Calphad* **2015**, *49*, 87-100.
 32. Woodcock, T. G.; Hermann, R.; Löser, W., Development of a metastable phase diagram to describe solidification in undercooled Fe-Co melts. *Calphad* **2007**, *31* (2), 256-263.
 33. Muralles, M.; Oh, J. T.; Chen, Z., Molecular dynamics study of FeCo phase transitions and thermal properties based on an improved 2NN MEAM potential. *Journal of Materials Research and Technology* **2022**, *19*, 1102-1110.
 34. Proffen, T.; Billinge, S.; Egami, T.; Louca, D., Structural analysis of complex materials using the atomic pair distribution function—A practical guide. *Zeitschrift für Kristallographie-Crystalline Materials* **2003**, *218* (2), 132-143.
 35. Billinge, S. J., The atomic pair distribution function: past and present. *Zeitschrift für Kristallographie-Crystalline Materials* **2004**, *219* (3), 117-121.
 36. Toby, B.; Egami, T., Accuracy of pair distribution function analysis applied to crystalline and non-crystalline materials. *Acta Crystallographica Section A: Foundations of Crystallography* **1992**, *48* (3), 336-346.
 37. Christian, J. W., *The theory of transformations in metals and alloys*. Newnes: 2002.
 38. Turnbull, D., Formation of Crystal Nuclei in Liquid Metals. *Journal of Applied Physics* **1950**, *21* (10), 1022-1028.
 39. Herlach, D. M., Containerless Undercooling and Solidification of Pure Metals. *Annual Review of Materials Science* **1991**, *21* (1), 23-44.

40. Perepezko, J. H.; Uttormark, M. J., Undercooling and nucleation during solidification. *ISIJ international* **1995**, 35 (6), 580-588.